AIP Journal of Applied Physics

# Luminescence enhancement by energy transfer in melamine-Y2O3:Tb3+ nanohybrids

Luigi Stagi, Daniele Chiriu, Andrea Ardu, Carla Cannas, Carlo M. Carbonaro, and Pier Carlo Ricci

Citation: Journal of Applied Physics **118**, 125502 (2015); doi: 10.1063/1.4931678
View online: http://dx.doi.org/10.1063/1.4931678
View Table of Contents: http://scitation.aip.org/content/aip/journal/jap/118/12?ver=pdfcov
Published by the AIP Publishing





# Luminescence enhancement by energy transfer in melamine-$Y_2O_3$:$Tb^{3+}$ nanohybrids

Luigi Stagi,[1,a)] Daniele Chiriu,[1] Andrea Ardu,[2] Carla Cannas,[2] Carlo M. Carbonaro,[1] and Pier Carlo Ricci[1]
[1]*Dipartimento di Fisica, Università degli Studi di Cagliari, S.P. Monserrato-Sestu Km 0,700, 09042 Monserrato (CA), Italy*
[2]*Departimento di Scienze Chimiche e Geologiche and INSTM, Università d Cagliari, SS 554 bivio Sestu, I-09042 Monserrato (CA), Italy*

(Received 15 July 2015; accepted 11 September 2015; published online 24 September 2015)

The phenomenon of luminescence enhancement was studied in melamine-$Y_2O_3$:Tb hybrids. Terbium doped $Y_2O_3$ mesoporous nanowires were synthesized by hydrothermal method. X-ray diffraction patterns and Raman scattering spectra testified the realization of a cubic crystal phase. Organic-inorganic melamine-$Y_2O_3$:$Tb^{3+}$ hybrid system was successfully obtained by vapour deposition method. Vibration Raman active modes of the organic counterpart were investigated in order to verify the achievement of hybrid system. Photoluminescence excitation and photoluminescence spectra, preformed in the region between 250 and 350 nm, suggest a strong interaction among melamine and Terbium ions. In particular, a remarkable improvement of $^5D_4 \rightarrow F_J$ Rare Earth emission (at about 542 nm) of about $10^2$ fold was observed and attributed to an efficient organic-Tb energy transfer. The energy transfer mechanism was studied by the use of time resolved photoluminescence measurements. The melamine lifetime undergoes to a significant decrease when adsorbed to oxide surfaces and it was connected to a sensitization mechanism. The detailed analysis of time decay profile of Terbium radiative recombination shows a variation of double exponential law toward a single exponential one. Its correlation with surface defects and non-radiative recombination was thus discussed. © *2015 AIP Publishing LLC*.
[http://dx.doi.org/10.1063/1.4931678]

## INTRODUCTION

The research on Rare Earth (RE) based materials is steadily active in order to realize new devices for photonic and optoelectronic applications requiring efficient light absorption, low losses of energy, and high quantum yield (QY) emission.[1,2] Several works on high band gap bulk material incorporating lanthanides ions report high quantum yield efficiency in the visible range.[3] Moreover, using an accurate co-doping and efficient interatomic energy transfer, metameric white light emission can be achieved.[4]

Yttrium oxide ($Y_2O_3$) has attracted much attention for its potential applications as a chemically and thermally stable host matrix.[5] Among its remarkable properties, it presents a high melting point of 2450 °C, high density (5.03 g cm$^{-3}$), and good thermal conductivity (33 Wm$^{-1}$ k$^{-1}$).[6] Furthermore, yttria based material can be adopted for photonic waveguide applications thanks to their high transmittance ranging from 280 nm to 8 $\mu$m and a refractive index of 2.[7]

Yttria energy gap of 5.5 eV favours a successful doping with several tripositive RE ions covering a wide range from blue to NIR. When doped with $Eu^{3+}$, it exhibits a red emission with a quantum yield of 92% for a bulk system (particles of $\sim$5 $\mu$m in size). The problem of quantum efficiency in RE doped $Y_2O_3$ at nanoscale has been addressed in several works, sometimes with controversial conclusions. In general, a reduction of QY is observed with decreasing size of nanoparticles depending on synthesis method and lowering of crystallinity.[8–10]

$Tb^{3+}$ ions has been considered as good candidate to cover the green region instead of $Er^{3+}$ and a codoping with $Yb^{3+}$ is frequently evaluated for upconversion applications.[11] Moreover, it has been showed a good efficient codoping-free upconversion process when irradiated with femtosecond sources.[12] However, the reduced photoluminescence (PL) quantum efficiency and, mainly, the deep UV excitation spectrum have strongly inhibited its use in $Y_2O_3$ doped crystal.

At nanoscale RE ions in oxide matrix rarely present a high quantum yield because of the high rate of non-radiative recombinations, caused by the defects at surfaces and the presence of $OH^-$ groups, mainly detrimental for IR emission.[9] Most recently, it was proposed to apply the synthesis strategy adopted for organic-RE complex in the field of nanostructured systems with encouraging results.[13] This approach consists in improving the luminescence of Rare Earth metals by organic ligands at the surfaces. This effect is known as "antenna effect" arising when light is strongly absorbed by organic ligand and much of the energy is then transferred to RE ions that emit efficiently.[14] Thanks to organic molecule, the obtained system can provide a good optical absorption even in region out of RE absorption resonance.[15]

In this work, we synthesized $Y_2O_3$:$Tb^{3+}$ nanostructures by hydrothermal method. Yttrium Hydroxides precursors are

a)Author to whom correspondence should be addressed. Electronic mail: luigi.stagi@dsf.unica.it. Phone: +39 0706754754. Fax:+39 0706753191.

 

first obtained and then a thermal treatment at high temperature yields the oxide nanocrystals. $Y_2O_3$:$Tb^{3+}$ were functionalised with 2,4,6-triamino-s-trazine (melamine) by thermal vapour method. Melamine ($C_3H_6N_6$) is known to have a strong absorption in UV region well matching with $Tb^{3+}$ ions absorption in several inorganic matrix. It also presents elevate thermal stability resulting a good candidate for high temperature synthesis methods. $Y_2O_3$:$Tb^{3+}$ pristine nanostructures (YTb) and their melamine-$Y_2O_3$:$Tb^{3+}$ (MeYTb) counterparts were analysed by steady state (SSPL) and time resolved photoluminescence (TRPL) to investigate the effect of organic presence at the surfaces and the mechanism behind the origin of $Tb^{3+}$ luminescence increase. The hybrid compound presents greatly enhanced luminescence for the green emission from $Tb^{3+}$ ions with excitation spectrum shifted trough the lower energy suggesting its potential application as phosphor in solid state lighting devices.

## EXPERIMENTAL SECTION

### Synthesis

All chemicals were purchased from Sigma-Aldrich and used without further purification. $Y_2O_3$ nanostructures (NS) were synthesized by surfactant tailored hydrothermal method. In a typical synthesis 1 g di $Y(NO_3)_3$*$6H_2O$ and 0,02 g of $Tb(NO_3)_3$*$5H_2O$ were dissolved in 10 ml of distilled water. Then, 0.5 ml of Diethanolamine (DEA) was added to the aqueous solution under vigorous stirring for 10 min. The solution was corrected at pH = 10 by means of a 10 M NaOH solution. The colloidal solution was transferred in a 50 ml Teflon-lined autoclave and hydrothermally treated at 180 °C for 24 h. After air quenching, the precipitate was washed with distilled water and dried at 60 °C in air for an hour. The hydroxide NS were calcinated at 600 °C for 3 h in air with a rate of 5 °C/min.

$C_3H_6N_6$ coated $Y_2O_3$ NS were prepared by thermal vapour deposition route. A certain amount of Melamine powder was put in an alumina crucible and Yttria NS were deposited on a silicon substrate at a distance of about 10 cm, placed in a quartz tube accommodated in tubular furnace and treated at 500 °C for 2h with 5 °C/min ramp under nitrogen flux (30 ml/min). Several samples with different melamine and $Y_2O_3$:$Tb^{3+}$ molar ratio ($n_{Me}$ / $n_{YTb}$) were synthesized in order to show dependence of luminescence enhancement on the organic concentration.

### Characterization techniques

The crystal structure of $Y_2O_3$:$Tb^{3+}$ samples was probed using X-ray diffraction patterns recorded by a Seifert X3000 diffractometer with a $\theta-\theta$ Bragg–Brentano geometry with Cu-K$\alpha$ wavelength. High resolution transmission electron microscopy (HRTEM) images were obtained by means of a JEM 2010 UHR equipped with a Gatan Imaging Filter (GIF) with a 15 eV window and a 794 slow scan CCD camera. The samples were dispersed in n-octane and submitted to an ultrasonic bath. Then, the suspensions were dropped on a copper grid covered with a carbon thin film for the observation.

In order to obtain information on the surface state of hybrid MeYTb samples, Raman spectra were acquired. Raman scattering measurements were performed in backscattering geometry at room temperature with a compact BWTEK i-Raman EX integrated system (spectral resolution of about 9 $cm^{-1}$) equipped with a microscopy system. The powders were irradiated with the 1064 nm line of a Nd:YAG laser.

For SSPL and Photoluminescence excitation (PLE) measurements was used the filtered light from a laser driven Xenon lamp (EQ-99-X) with a final bandwidth of about 1 nm.

TRPL measurements were performed using an optical parametric oscillator with a frequency doubler device, pumped by the third harmonic (355 nm) of a pulsed Nd:YAG laser (Quanta-Ray Pro 730). The excitation pulse width at half-maximum was 8 ns with 10 Hz of repetition rate, and spectral bandwidth less than 0.3 $cm^{-1}$. The PL signal was dispersed by a spectrograph (ARC-SpectraPro 300i) with a spectral bandpass <2.5 nm and detected by a gateable intensified CCD (PI MAX Princeton Inst.).

## RESULTS AND DISCUSSION

Fig. 1 reports the representative XRD pattern of the hydrothermal synthesized samples, annealed at the temperature of 600 °C, acquired in the Bragg angles range $16° \leq 2\theta \leq 65°$. As prepared samples show a sequence of broadened reflections assignable to the nanostructured cubic bixbyite-like phase with peaks indexed by PDF-Card 83-0927. No other phases were detected and all diffraction peaks are attributed to *Ia-3* space group (No. 206) with no deviation caused by impurity elements from the pure phase. The related crystal parameters are shown in Table I. It is worth to note the large value of the strain parameter, determined by the relation $\varepsilon = \beta\cos\theta/4$, especially when compared with the ones previously reported on 40–60 nm nanoparticles.[16] This result can be reasonably assigned to an increase of atomic displacements in correspondence of grain boundary, frequently observed in small oxide nanosystems or in particles with highly porous surfaces.[17]

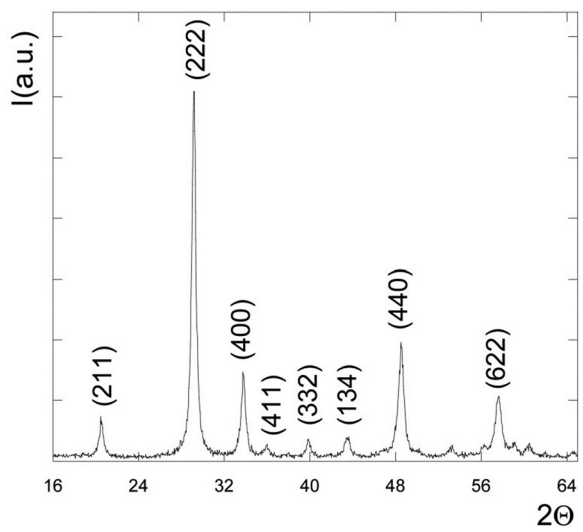


FIG. 1. XRD pattern for $Y_2O_3$:$Tb^{3+}$ sample.

TABLE I. Crystal Parameter of $Y_2O_3$:$Tb^{3+}$ nanostructure.

| Structural parameters | Calculated values |
|---|---|
| $2\theta$ | 29.10 |
| FWHM (deg) | 0.45 |
| Microstrain $\varepsilon(10^{-3})$ | 1.92 |
| Lattice constant (Å) | 10.62 |
| Interplanar spacing (Å) | 3.066 |

TEM and high resolution (HRTEM) images of the untreated $Y_2O_3$:$Tb^{3+}$ sample are reported in Fig. 2. As shown, the hydrothermal product consists of relatively dispersed elongated nanostructures with predominantly tubes features. The outer diameter was estimated of 100 nm and the length of about 1 $\mu$m. Beside a certain homogeneity in shape and dimension, the most relevant result concerns the porous characteristics in accordance with the hypothesis assumed for diffraction patterns.

Below the temperature of 1000 °C, Rare Earth sesquioxides crystallize in bixbyite-like cubic structure whose corresponding irreducible representation for the vibrational optical modes is

$$\Gamma_{opt} = 4A_g + 4E_g + 14F_g + 5A_{2u} + 5E_u + 16F_u, \quad (1)$$

and therefore, it accounts for 22 Raman $(A_g, E_g, F_g)$ and 16 IR $(F_u)$ active modes.

In a typical sesquioxides scattering spectrum, we distinguish the frequencies region above 300 $cm^{-1}$, weakly influenced by Rare Earth ions and ascribable to oxygen motions and deformation of $ReO_6$ octahedra. O-Re-O and Y-O-Y bending mainly affect the lowest frequencies and Y-O stretching the higher ones.[18]

Raman spectra of $Y_2O_3$:$Tb^{3+}$ and melamine-$Y_2O_3$:$Tb^{3+}$ samples are shown in Fig. 3, and the respective assignments are summarized in Table II.

$Y_2O_3$ nanotubes Raman spectrum is dominated by $F_g$ mode at 376 $cm^{-1}$ rising from $Y^{3+}$-$O^{2-}$ vibration.[19] According to the most recent attributions, we identify the $F_g$ modes at 468 and 592 $cm^{-1}$.[20] Furthermore, adjacent to the most intense contribution, we recognise two not completely resolved vibrations at 329 and 429 $cm^{-1}$ attributed to $F_g + E_g$ and $A_g$ modes, respectively.[20]

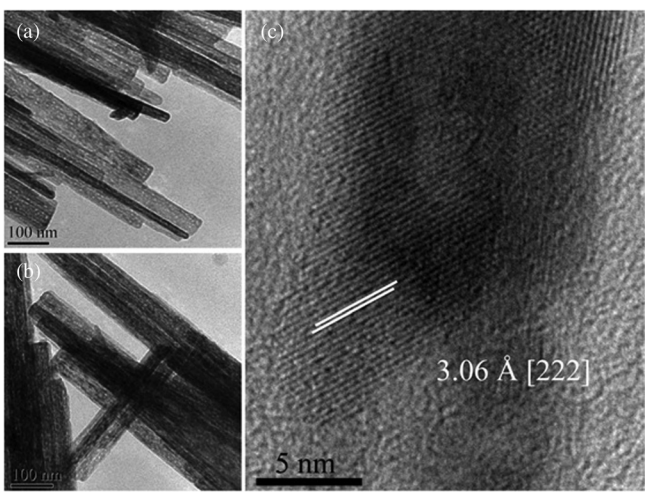


FIG. 2. TEM (a) and (b) and HRTEM (c) images of $Y_2O_3$:$Tb^{3+}$ nanostructures.

The organic functionalised sample presents new features at 700 and 990 $cm^{-1}$ that could be attributed to the melamine (Fig. 3(b)). Taking into account the melamine Raman spectrum (Fig. 4), two intense modes are individuated at 675 $cm^{-1}$ and 983 $cm^{-1}$, originating from the ring breathing II mode and in-plane ring breathing I mode, respectively.[21] Raman modes at wavenumbers lower than 600 $cm^{-1}$ typically belong to N-$H_2$ (not observed in this work) and H-N-C-N stretching. The mode at 778 $cm^{-1}$ and the peaks' couple at 1443 and 1556 $cm^{-1}$ are due to out of plane N-C-N bending and C-N stretching, respectively[21] (see Table II for the complete attribution).

$D_{3h}$ symmetry based carbon-nitrogen compounds, including melamine and melem (2,4,6-triamino-tri-s-triazine), can present a marked N-donor behaviour; melamine, especially, can produce Cu or Ag-based complex through the nitrogen atom of the aromatic ring. Conversely, it was proposed a strong interaction of melamine with gold surfaces through amino group in SERS experiments. The latter is motivated by a significant redshift of the mode at 675 $cm^{-1}$ but not the one at 983 $cm^{-1}$.[22]

Raman measurements on the hybrids melamine-yttria show a shift toward higher wavenumbers of about 25 $cm^{-1}$ for the ring breathing II mode and only 7 $cm^{-1}$ for the ring breathing I mode. In the light of this, we suggest chelation to the amine group's nitrogen atoms as the most likely mechanism, without significant involving of the ring N atoms.

Fig. 5 shows the resulting excitation spectra (PLE) of melamine, $Y_2O_3$:$Tb^{3+}$ and melamine-$Y_2O_3$:$Tb^{3+}$ hybrid. Monitoring the characteristic emission of melamine powder in the UV region, the excitation spectrum reveals a structured broad band with a maximum at 312 nm (Fig. 5(a)). At the present, we do not have knowledge of melamine excitation spectra to compare with our results, but several works on the absorption of melamine in solution were already published.[23–25] According to Dewar and Paolini,[23] the main absorption band of melamine in solution of water and ethanol is dominated by a singlet-singlet transition around 240 nm with a weak shoulder at 313 nm attributed to a singlet-triplet excitation. Most recently, fluorescence excitation spectra of melamine in water show the main excitation peak at 254 nm, with a weak contribution in the region between 260 and 320 nm.[24] Our starting powder present similar excitation features to the ones appearing in PLE measures on melamine powder after treatment at 300 °C showing a broad excitation band extending from 260 nm to 400 nm as a product of a condensation process.[25]

Melamine luminescence exhibits an efficient emission picked at 356 nm and ~60 nm wide, with a long tail extending in the blue range, mainly originated by triplet-ground state recombination.[24]

The main excitation channels of Terbium ions in yttrium oxide matrix are located at energies higher than 320 nm, optimally overlapping the excitation features of melamine molecule. PLE spectrum of $Y_2O_3$:$Tb^{3+}$, reported in Fig. 5(b), is acquired by monitoring the emission band centred at

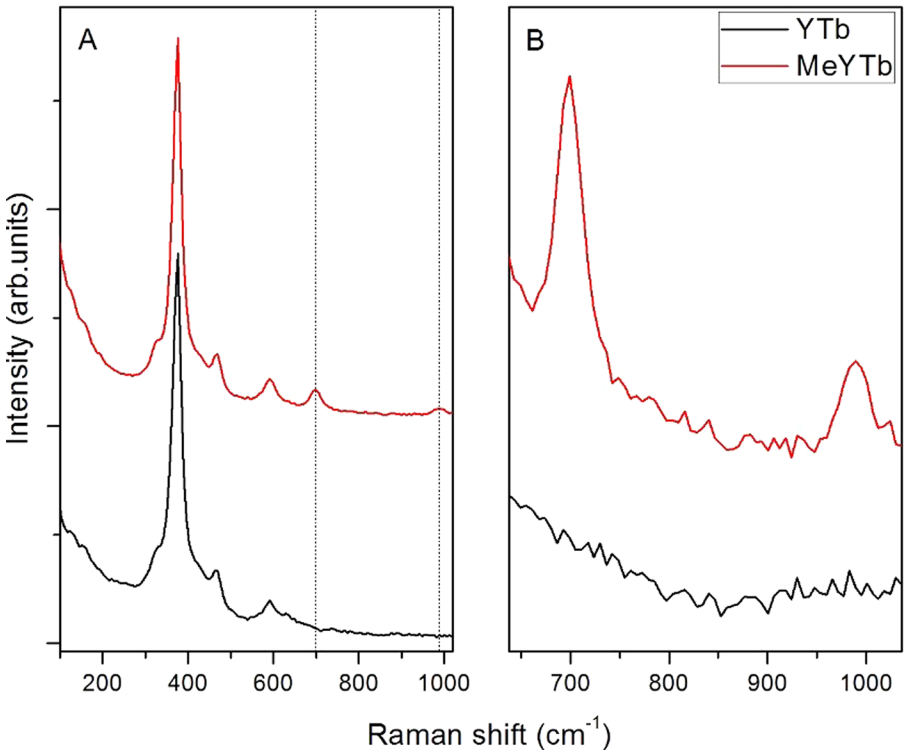


FIG. 3. Raman spectra of $Y_2O_3:Tb^{3+}$. (a) Extended Raman spectra. (b) Particular of Raman spectra at 640–1036 $cm^{-1}$.

542 nm. The continuum band picked at about 290 nm is ascribable to 4f-5d intraband transitions that are recognized to be largely dependent on crystalline environment or crystallite dimensions in nanoparticles systems.[26] The corresponding luminescence showing a group of four sharp bands is observed, namely, 484 nm (J = 6), 542 nm (J = 5), 583 nm(J = 4), and 617 nm (J = 3) in the region between 450 nm and 650 nm, all attributed to $^5D_4 \rightarrow F_J$ terbium ions radiative recombinations.

MeYTb hybrid (with molar ratio $n_{Me}/n_{YTb} = 2$) is characterized by a strong green luminescence displaying the characteristic bands of terbium ions combined with the emission of melamine (Fig. 5(c)). The excitation spectrum of MeYTb recorded at the Tb emission (542 nm) presents the distinctive feature of melamine with an asymmetric broad band picked at about 310 nm, emblematic of a marked interaction between organic compound and lanthanide ion.

Focusing on melamine photoluminescence, a variation in the PL spectrum is observed. As shown in Fig. 6, when melamine is adsorbed at yttria surfaces (sample MeYTb) the emission peak is redshifted to 370 nm. This behaviour is in accordance with the one observed in Pr(III)-phenanthroline and RE(III)-melamine complex.[27,28] Particularly in the latter, the energy related to $\pi \rightarrow \pi^*$ radiative transition can be significant affected by organic-metal coordination causing a redshift of about 12 nm from the intrinsic value.[28]

The shift toward lower energies of the melamine emission strongly represents an experimental evidence of the

TABLE II. Raman assignments of YTb, MeYTb and Melamine samples.

| YTb | MeTb | Attribution |
|---|---|---|
| 329 | | $F_g + E_g$ |
| 376 | | $F_g$ |
| 429 | | $A_g$ |
| 468 | | $F_g$ |
| 592 | | $F_g$ |
| | 700 | Ring breathing II mode |
| | 990 | Ring breathing I mode |
| **Melamine** | | **Attribution** |
| 233 | | HNCN torsion |
| 383 | | HNCN torsion |
| 450 | | HNCN torsion |
| 586 | | Out of plane CNC bending |
| 675 | | Ring breathing II mode |
| 778 | | Out of plane NCN bending |
| 983 | | Ring breathing I mode |
| 1443 | | CN stretching |
| 1556 | | CN stretching |

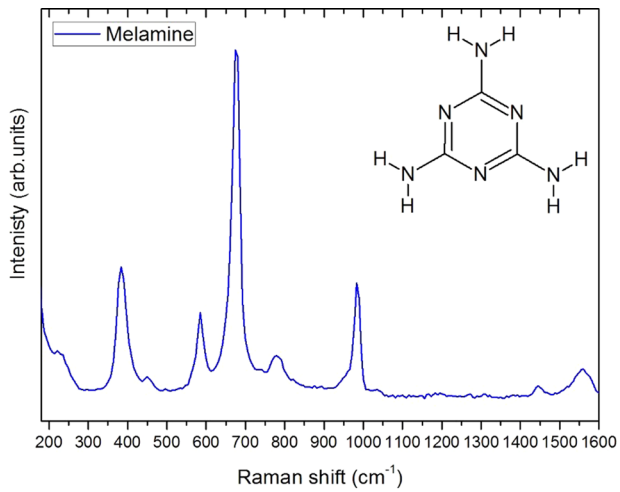


FIG. 4. Raman spectrum of melamine.

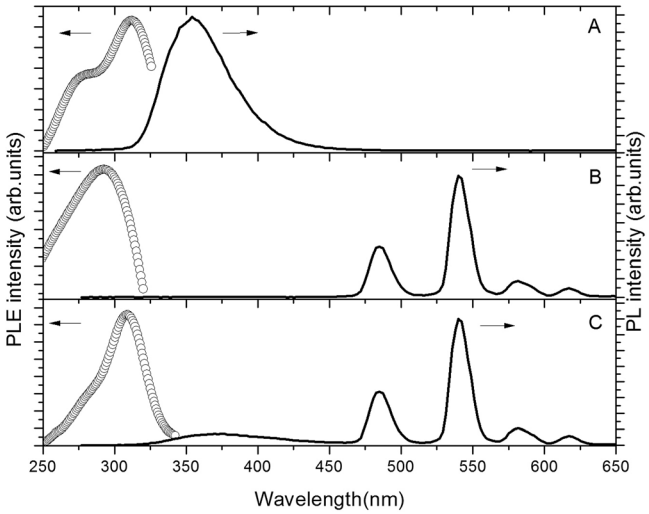


FIG. 5. Photoluminescence excitation (circles) and photoluminescence (solid line) spectra of Melamine (A, $\lambda_{em} = 360$ nm, $\lambda_{exc} = 270$ nm), YTb (B, $\lambda_{em} = 542$ nm, $\lambda_{exc} = 290$ nm) and MeYTb(C, $\lambda_{em} = 542$ nm, $\lambda_{exc} = 290$ nm).

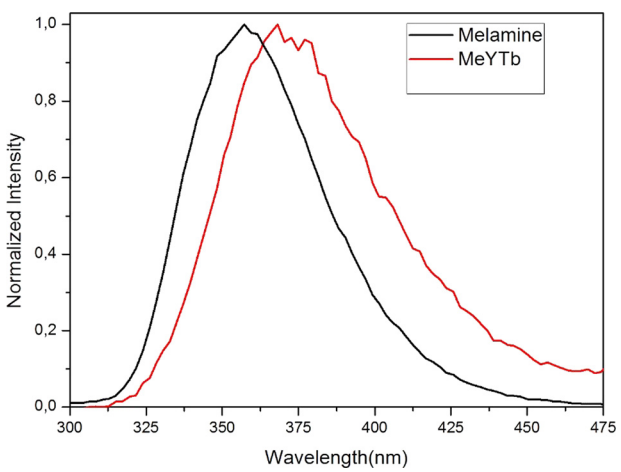


FIG. 6. Melamine photoluminescence spectrum excited at 270 nm.

successful coordination among organic ligand and Rare Earth ions at the surfaces, in good agreement with hybrid Raman spectra characteristics.

In the composite organic-inorganic system, the lanthanide emission is governed by the relation

$$I^*_{RE} = \eta(\lambda_{exc}) I_{RE}, \tag{2}$$

in which we recognize the sensitization of Rare Earth (RE) ions by organic ligand in the form of intrinsic luminescence $I_{RE}$ improvement. $\eta$ is the increase factor and it will be dependent on excitation wavelength. In Fig. 7(a) we report a representative sketch of $\eta$ defined as the ratio $I^*_{Tb}/I_{Tb}$ of the emission intensities at 542 nm ($^5D_4 \rightarrow F_5$). The factor $\eta$ reaches the highest value with excitation wavelength of about 300 nm, where $\eta \sim 150$. In the range between 250 and 320 nm, we observe a luminescence improvement of one order of magnitude at least. $\eta$ curve essentially follows the excitation spectrum of melamine with $\eta > 10^2$ for $\lambda_{exc} > 300$ nm where excitation spectrum is dominated by the organic feature. Fig. 7(b) shows the progressive increase of $\eta$ with the concentration of melamine. Above $n_{Me}/n_{YTb} = 0.3$, the maximum value of Tb luminescence is detected and it remains constant on a wide range.

Time resolved measurements in the scale of ms were performed in order to investigate possible effect of organic capping on $Tb^{3+}$ ions radiative recombinations (Fig. 8). For this purpose, the most intense band at 542 nm was monitored in the first 2 ms. As expected, $^5D_4 \rightarrow F_5$ of $Tb^{3+}$ in $Y_2O_3$ presents a lifetime of several hundred $\mu$s. By an accurate comparison between the two samples, we observe a significantly difference in radiative decay. In general, $Y_2O_3$:$Tb^{3+}$ photoluminescence presents two well-defined lifetimes and the decay profile follows a bi-exponential law:[12]

$$I(t) = I_1 \exp\left(-\frac{t}{\tau_1}\right) + I_2 \exp\left(-\frac{t}{\tau_2}\right), \tag{3}$$

with

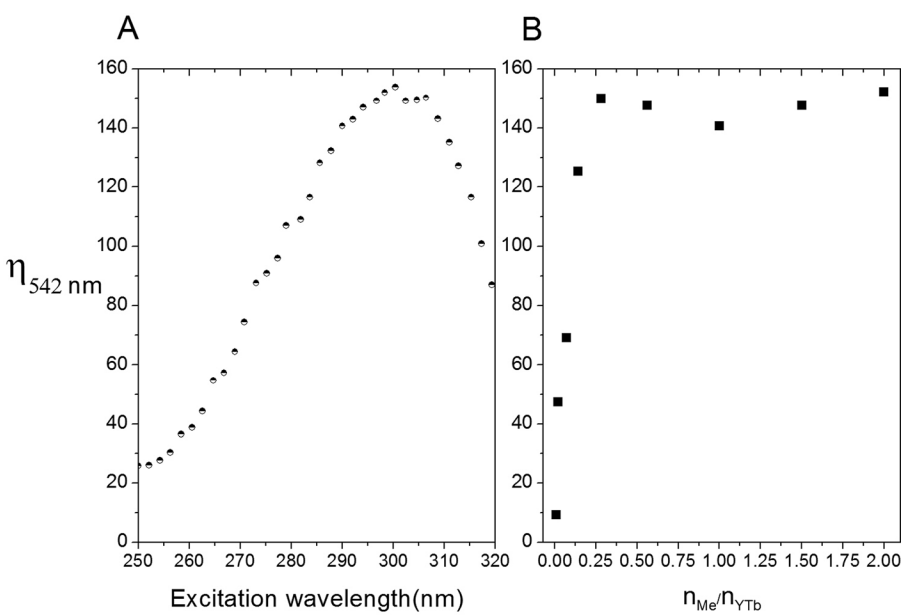


FIG. 7. (a) $\eta_{eff}$ parameter in the range 250–320 nm; (b) $\eta_{eff}$ parameter as a function of molar ratio $n_{Me}$ / $n_{YTb}$.

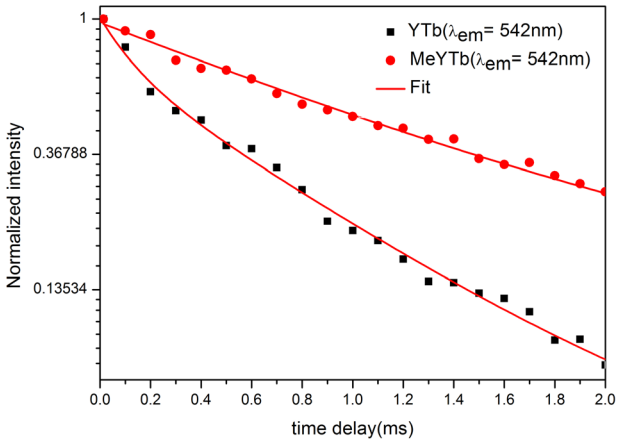


FIG. 8. Normalized luminescence decay at 542 nm of YTb (black dots) and MeYTb (red dots), $\lambda_{exc} = 270$ nm.

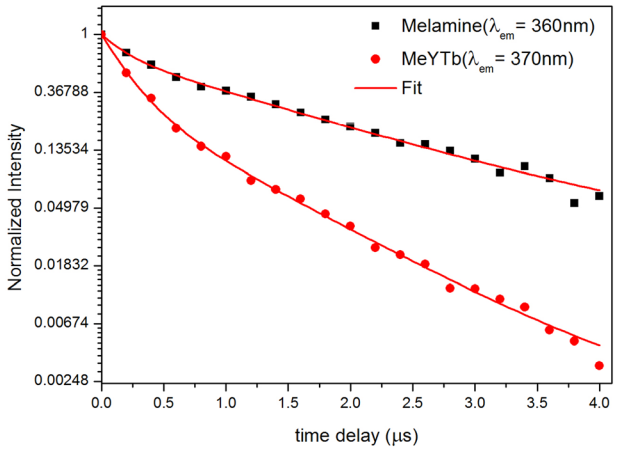


FIG. 9. Normalized luminescence decay of melamine (black dots) and melamine in MeYTb (red dots), $\lambda_{exc} = 270$ nm.

$$\frac{1}{\tau} = \frac{1}{\tau_r} + \frac{1}{\tau_{nr}}, \tag{4}$$

where $\tau_r$ and $\tau_{nr}$ represent radiative and non-radiative lifetime contribution to the overall time decay $\tau$.[12]

Pristine $Y_2O_3$:$Tb^{3+}$ nanostructured luminescence can be fitted with two exponentials with lifetimes $\tau_1 = 0.13$ ms and $\tau_2 = 0.78$ ms (all expressed with an accuracy of 5%). Multiexponential trend of terbium luminescence decay has been encountered in several works, especially in $Gd_2O_3$:Tb systems.[29,30] The effect is always correlated to the energy dissipation by the presence of non-radiative recombination channels, mainly represented by other lanthanide ions whose levels can be populated by efficient interionic transfer and drastically increase with the doping concentration.[31] Moreover, structural defects and unsaturated bonds are always present at oxide surfaces whom tend to react with water and favour the formation of metal-hydroxides sites.[32] Hydroxyl group contribution became more important as the particles size decreases promoting non-radiative recombination paths, frequently observed in faster components during luminescence decays. The use of inorganic or organic shell can prevent this deleterious mechanism, separating the optical active core from OH-groups influence. Terbium ions deposited on porous anodic $Al_2O_3$ shows a strong luminescence quenching, related to non-radiative conversion in OH-groups vibration energies. It has been demonstrated that high temperature (>900 °C) annealing process can decrease the amount of OH species at the surfaces achieving an improvement of terbium ions luminescence.

Defining the average time as[12]

$$\tau^* = \frac{I_1\tau_1^2 + I_2\tau_2^2}{I_1\tau_1 + I_2\tau_2} \tag{5}$$

and applying it to the luminescence decay in YTb sample, we obtain $\tau^* = 0.73$ ms. On the other hand, the photoluminescence decay of MeYTb nanostructures can be fitted with a single exponential with lifetime $\tau = 1.25$ ms, resulting in an improvement (considered with respect to the average time of YTb) of about 70%.

We argue that naturally hydrated surfaces undergo to hydroxyl groups desorption during the heat treatment at 500 °C under nitrogen flux. The resulting surfaces present high density of reactive centres involved in melamine adsorption. Melamine molecules tend to heal unsaturated bonds when deposited at high temperature on the yttria surface, influencing the dynamic of lanthanide ions recombinations. In this scenario, non-radiative contribution lessened, and so the $\tau_{nr}$, causing the increase of terbium lifetime emission. Dorman *et al.* observed similar behaviour on $Y_2O_3$:$Er^{3+}$ nanoparticles passivated by an inert shell with an optimal size of about 8 nm. The nanoparticles display enhanced luminescence and a longer luminescence lifetime with an improvement of 53%.[33]

To clarify the mechanism of energy transfer in melamine-Rare Earth complex is necessary to investigate the time evolution of the organic molecule luminescence. In Fig. 9, we monitored the integrated luminescence of melamine in powders and coordinated to yttria nanostructures. As previously reported, the decay profile of melamine fluorescence exhibits two lifetimes, a fast component of 200 ns and the other with a lifetime of 1.5 $\mu$s, highly dependent on chemical environment. Accordingly, the interaction among adsorbed melamine and surfaces' ions induce the lowering of the slowest lifetime down to 860 ns (Table III).

The main effect originating from the obtained hybrid melamine-$Y_2O_3$:$Tb^{3+}$ nanostructure is an increase of doping ions luminescence efficiency. The reduced energy gap between melamine transition (resonant absorption condition) and $Ln^{3+}$ levels promotes an efficient energy transfer corresponding to a gain of about one order of magnitude. In agreement with the most accepted mechanism, the organic donor, excited in the range between 250 and 320 nm, undergoes to a first singlet

TABLE III. Optical emitters Lifetimes.

| Emitter | YTb $\tau_1$ / $\tau_2$ (ms) | MeYTb $\tau_1$ / $\tau_2$ (ms) | Melamine $\tau_1$ / $\tau_2$ ($\mu$s) |
|---|---|---|---|
| $Tb^{3+}$($\lambda_{em} = 542$ nm) | 0.13 / 0.78 | 1.25 | - |
| Melamine | - | $2.0 \times 10^{-4}$ / $8.6 \times 10^{-4}$ | 0.2 / 1.5 |

state transition and relaxes to a triplet state through intersystem crossing. Then part of energy is transferred to $D_4$ levels of terbium ion which recombines with intense luminescence.

## CONCLUSIONS

Terbium doped $Y_2O_3$ nanostructures were synthesized by hydrothermal method and annealing at 600 °C. The resulting powders display porous surfaces facilitating the anchoring and adsorption of ligand molecules. Consequently, a functionalization of oxide surfaces with melamine has been obtained by thermal deposition method under nitrogen flux at 500 °C preventing the polymerization of organic ligand. The achieved hybrid exhibits a strong luminescence in the green region with an improvement of efficiency compared with pristine sample. This result can be explained in the framework of an energy transfer between melamine and RE ions and it is confirmed by the reduced lifetime of melamine emission. Moreover, the increase of $Tb^{3+}$ lifetime suggests the removal of surface defects and related optical quenchers in the presence of organic ligand. High temperature synthesis of melamine-oxide hybrids compounds favours an $OH^-$ free strategy to obtain an effective improvement of lanthanides based nanoscaled phosphors.

## ACKNOWLEDGMENTS

L.S. gratefully acknowledges Sardinia Regional Government for the financial support of his Ph.D. scholarship (P.O.R. Sardegna F.S.E. Operational Programme of the Autonomous Region of Sardinia, European Social Fund 2007–2013–Axis IV Human Resources, Objective l.3, Line of Activity l.3.1.).

[1]Y. Hagesawa and T. Nakanishi, RSC Adv. **5**, 338 (2015).
[2]Z. Yang, H. Wu, J. Li, B. Shao, J. Qiu, and Z. Song, J. Alloys Compd. **641**, 127 (2015).
[3]P. Gorrotxategi, M. Consonni, and A. Gasse, J. Solid State Light **2**, 1 (2015).
[4]X. Zhang, L. Zhou, Q. Pang, J. Shi, and M. Gong, J. Phys. Chem. C **118**, 7591 (2014).
[5]C. Cannas, M. Casu, A. Lai, A. Musinu, and G. Piccaluga, PCCP **4**, 2286 (2002).
[6]T. Gougousi and Z. Chen, Thin Solid Films **516**, 6197 (2008).
[7]H. Guo, W. Zhang, L. Lou, A. Brioude, and J. Mugnier, Thin Solid Films **458**, 274 (2004).
[8]A. van Dijken, J. Makkinje, and A. Meijerink, J. Lumin. **92**, 323 (2001).
[9]M. A. A. Attia, S. Garroni, D. chiriu, C. Ricci, F. Delogu, R. Orrù, and G. Cao, Chem. Phys. Lett. **618**, 108 (2015).
[10]C. Cannas, M. Casu, A. Musinu, G. Piccaluga, A. Speghini, and M. Bettinelli, J. Non-Cryst. Solids **306**(2), 193 (2002).
[11]H. J. Liang, G. Y. Chen, L. Li, Y. Liu, F. Quin, and Z. G. Zhang, Opt. Commun. **282**, 3028 (2009).
[12]Q. Lü, Y. Wu, L. Ding, G. Zu, A. Li, Y. Zhao, and H. Cui, J. Alloys Compd. **496**, 488 (2010).
[13]L. Ji, N. Chen, G. Du, M. Yan, and W. Shi, Ceram. Int. **40**, 3117 (2014).
[14]A. Ishii and M. Hasegawa, Sci. Rep. **5**, 11714 (2015).
[15]J.-C. Bünzli and C. Piguet, Chem. Soc. Rev. **34**, 1048 (2005).
[16]S. Som and S. K. Sharma, J. Phys. D: Appl. Phys. **45**, 415102 (2012).
[17]Y. H. Zhao, K. Zhang, and K. Lu, Phys. Rev. B **56**, 14322 (1997).
[18]Y. Repelin, C. Proust, E. Husson, and J. M. Beny, J. Solid State Chem. **118**, 163 (1995).
[19]J. Q. Xu, S. J. Xiong, X. L. Wu, T. H. Li, J. C. Shen, and P. K. Chu, J. Appl. Phys. **114**, 093512 (2013).
[20]M. V. Abrashev, N. D. Todorov, and J. Geshev, J. Appl. Phys. **116**, 103508 (2014).
[21]M. Prabhaharan, A. R. Prabhaharan, S. Gunasekaran, and S. Srinivasan, Spectrochim. Acta Part A **123**, 392 (2014).
[22]A. Kim, S. J. Barcelo, R. S. Williams, and Z. Li, Anal. Chem. **84**, 9303 (2012).
[23]M. J. S. Dewar and L. Paolini, Trans. Faraday Soc. **53**, 261 (1956).
[24]C. Yang, Y. Liu, and F. Zhang, Spectrochim. Acta Part A **75**, 1329 (2010).
[25]Y. Zhang, Q. Pan, G. Chai, M. Liang, G. Dong, Q. Zhang, and J. Qiu, Sci. Rep. **3**, 1 (2013).
[26]Y. L. Soo, S. W. Huang, Z. H. Ming, and Y. H. Kao, J. App. Phys. **83**, 5404 (1998).
[27]M. Hasegawa, A. Ishii, and S. Kishi, J. Photochem. Photobiol. **178**, 220 (2006).
[28]M. Hasegawa, A. Ishii, K. Habu, H. Ichikawa, K. Maeda, S. Kinshi, and Y. Shigesato, Sci. Technol. Adv. Mater. **7**, 72 (2006).
[29]B. Mutelet, P. Perriat, G. Ledoux, D. Amans, F. Lux *et al.*, J. Appl. Phys. **110**, 094317 (2011).
[30]C. Louis, S. Roux, G. Ledoux, C. Duajadin, O. Tillement, B. L. Cheng, and P. Perriat, Chem. Phys. Lett. **429**, 157 (2006).
[31]P. C. Ricci, M. Salis, R. Corpino, C. M. Carbonaro, E. Fortin, and A. Anedda, J. Appl. Phys. **108**, 043512 (2010).
[32]L. Stagi, J. A. De Toro, A. Ardu, C. Cannas, A. Casu, S. S. Lee, and P. C. Ricci, J. Phys. Chem C **118**, 2857 (2014).
[33]J. A. Dorman, J. H. Choi, G. Kuzmanich, J. R. Bargar, and J. P. Chang, J. Phys. Chem C **116**, 10333 (2012).